Journal of Power Sources 196 (2011) 9757–9766

Contents lists available at ScienceDirect

Journal of Power Sources

journal homepage: www.elsevier.com/locate/jpowsour

Modeling the capacity degradation of $LiFePO_4$/graphite batteries based on stress coupling analysis

Zhe Li [a], Languang Lu [a], Minggao Ouyang [a,*], Yuankun Xiao [b]

[a] State Key Laboratory of Automotive Safety and Energy, Tsinghua University, Beijing 100084, PR China
[b] Delta Electronics, Inc, Shanying Road 252, Guishan Industrial Park, Taoyuan County, Taiwan

ARTICLE INFO

Article history:
Received 15 May 2011
Received in revised form 4 July 2011
Accepted 26 July 2011
Available online 4 August 2011

Keywords:
$LiFePO_4$ battery
Capacity degradation
Stress coupling

ABSTRACT

A coupling-analysis-based model to predict the capacity degradation of $LiFePO_4$ batteries under multi-stress accelerated conditions has been developed. In this model, the joint effect on the battery capacity degradation of any 2 out of 5 stress factors, which include ambient temperature, end of discharge and charge voltage (EODV and EOCV), and discharge and charge rate, is studied through coupling validation tests. Coupling generally exists among these 5 stress factors, and the coupling intensity has a certain relationship with the stress levels. There is a critical stress level at which the coupling can be considered negligible, and when the stress level goes higher, coupling aggravates battery degradation exponentially. Additionally, the study also indicates that battery life shows stronger sensitivity to discharge rate and EOCV than to charge rate and EODV. The developed capacity degradation model based on the input of real operating conditions and coupling intensity calibration achieves error less than 15% when the cycling goes into the stable decay period, and the error converges gradually as the cycling continues.

1. Introduction

Battery degradation is generally predicted using one of two approaches [1,2]. The first one is based on electrochemical models [3,4] and focuses on the micro-mechanism of battery degradation on both positive [5,6] and negative electrodes [7–9], such as active particle loss, metal sediment or SEI film accumulation [10–13].

The other approach was developed to describe experimental phenomena, like capacity fade and resistance increase, by fitting the cycling data [14–16]. Instead of investigating the sophisticated internal electrochemical principles of battery cycling, the second approach avoids the recognition of battery design or manufacturing parameters, and only external characteristics, which can be measured easily, are required.

For the second prediction method, a significant amount of research has focused on the effect of DOD (depth of discharge), discharge rate, EODV or EOCV on the battery lifespan, but most results have been described roughly by experimental curves of the capacity fade or increase in resistance. Only a few mathematical models have been extracted and established. The most widely used external characteristics model represents the law between ambient temperature and cycling capacity loss [17,18]. Although an Ah-throughput model [19] takes the coupling effect of temperature and discharge rate into account, the other models are mostly single stress accelerated; moreover, the models do not account for the existence of coupling between different stresses.

Therefore, these models are not necessarily accurate when applied to cycle degradation prediction under complex real running conditions; for instance, under real road conditions for electric vehicles.

In this paper, our proposed model has several new features: first, the most important factors that affect battery degradation, i.e., temperature, EODV, EOCV, discharge rate and charge rate, are all adopted as the stresses and are used as the input to the model. Second, the coupling law between these stresses is studied and quantified by a long-term coupling validation test. Finally, a capacity degradation model based on stress coupling analysis is established with error evaluation and factor sensitivity analysis.

2. Experiment design

The coupling validation test is carried out as follows. In the first part, a single stress is accelerated, whereas others are set to the standard stress levels defined in Table 1. The impact of that single factor on battery degradation is evaluated based on life characteristics, such as the capacity fade and resistance increase. In the second part, two factors are adjusted simultaneously to accelerated levels, and the life characteristics of the experimental results are compared to the results in the first part. If the capacity fade rate in the two-factor accelerated test was similar to the sum of the rates in

* Corresponding author. Tel.: +86 10 62792797; fax: +86 10 62789699.
E-mail address: ouymg@tsinghua.edu.cn (M. Ouyang).

0378-7753/$ – see front matter © 2011 Elsevier B.V. All rights reserved.
doi:10.1016/j.jpowsour.2011.07.080

Table 1
Standard levels of 5 factors.

	Temperature	Discharge rate	EODV	Charge rate	EOCV
Standard levels	30 °C	1/3 C	2 V	1/3 C	3.65 V

the two corresponding single-factor accelerated tests, the coupling between these two factors can be ignored, i.e., these two factors are almost decoupled. If they are quite different, it can be determined that there is strong, non-negligible coupling between the two factors, and a further probe into the relationship between the coupling factors is required to reveal the strength of the coupling and to represent the coupling law in the capacity degradation model.

The ambient temperature, discharge rate, EODV, charge rate and EOCV are selected as the input stresses. The overall durability test procedures are as follows. First, the single-factor and two-factor tests are performed to acquire the fade rate of capacity and the increase in resistance, to validate the existence of coupling between the two factors and to explore the relationship between the coupling intensity and stress levels. Second, several groups of single-factor acceleration tests with different stress levels are performed to identify the parameters in single-stress accelerated models. Third, using single-stress accelerated models and the coupling intensity laws, the capacity degradation model is derived taking into account the coupling between factors. Finally, the model accuracy is verified experimentally, and the factor sensitivity of this model is analyzed.

The following criteria are determined for all the cycles in the test:

(1) The battery capacity fade: A standard battery capacity test method is adopted to ensure the comparability between the capacity fade rates under different cycle conditions. The standard battery capacity test has the following parameters: a fixed room temperature, the standard charging method (see (3) below) charged to full, rest for 1 h, then 1/3 C constant discharge to a cut-off voltage of 2.0 V.
(2) The frequency of the standard capacity test: After every 20 cycles (i.e., after cycle 20, 40, 60, 80, . . .), the battery is switched to room temperature and gets a rest of 12 h, and the standard capacity and the DC resistance of the battery are measured under 1/3 C constant discharge.
(3) Charging method: In each cycle, the charge rate and EOCV are chosen in accordance with the experimental conditions shown in Tables 3 and 4 using the CC–CV (constant-current, constant voltage) method. The constant voltage charging stage stops when the current drops to 1/10 of the constant charging current. The constant current and EOCV of the charging in the standard capacity test are 1/3 C and 3.65 V.
(4) Rest time between adjacent cycles: 5 min in general. However, in the experimental results shown in Fig. 4(a), because the cycle capacity declines rapidly due to harsh cycling conditions, the rest time is changed from 5 min to 2 h, and the adjustment point is shown in the figure.
(5) When to stop cycling: Cycling continues until one of the following occurs: the standard battery capacity drops to 60% of the nominal capacity, the cycling capacity drops to 15% of the nominal capacity, a total of 200 cycles is completed, or unsafe circumstances occur, such as battery bulging or a sharp rise in temperature.
(6) Temperature adjustment: After the adjustment of the ambient temperature, the battery should first rest for more than 12 h until the internal and external temperatures coincide.
(7) Resistance test method: HPPC test [20] with a pulse current of 1 C.

Table 2
The parameters of the subject battery.

Items	Parameters and units
Nominal capacity	11 Ah
Nominal voltage	3.2 V
Weight	≤400 g
Size	27(+1.5, −0) mm × 70(±0.2) mm × 104(±0.4) mm

Table 3
Single factor accelerated experiments.

Test No.	Temperature	Discharge rate	EODV	Charge rate	EOCV
1–1	45 °C	[a]			
1–2		4 C			
1–3			1.25 V		
1–4				1.5 C	
1–5					3.95 V

[a] The blanks refer to 'standard stress levels' from Table 1; the same system is used below.

2.1. Single factor accelerated experiments

The experiments were performed on some new $LiFePO_4$/graphite cells and the parameters of the battery are shown in Table 2. For all the experiments in Table 3, only one stress is accelerated, and the others remain at the standard levels shown in Table 1.

2.2. Double-factor accelerated experiments

The experiments were carried out on 10 cells of the same kind as those in Section 2.1. Each of the experiments has double accelerated

Table 4
Double-factor accelerated experiments.

Test No.	Temperature	Discharge rate	EODV	Charge rate	EOCV
2–1	45 °C	4 C			
2–2	45 °C		1.25 V		
2–3	45 °C			1.5 C	
2–4	45 °C				3.95 V
2–5		4 C	1.25 V		
2–6		4 C		1.5 C	
2–7		4 C			3.95 V
2–8			1.25 V	1.5 C	
2–9			1.25 V		3.95 V
2–10				1.5 C	3.95 V

Table 5
The calculation of coupling error.

Single stress				Corresponding double stress		Coupling error Δ (%)
Test No.	SCFR	Test No.	SCFR	Test No.	$SCFR_d$	
1–1	0.00576	1–2	0.01425	2–1	0.02025	−1.19
1–1	0.00576	1–3	0.00543	2–2	0.00527	112.33
1–1	0.00576	1–4	0.00474	2–3	0.00798	31.58
1–1	0.00576	1–5	0.00481	2–4	0.00535	97.57
1–2	0.01425	1–3	0.00543	2–5	0.02221	−11.39
1–2	0.01425	1–4	0.00474	2–6	0.02065	−8.04
1–2	0.01425	1–5	0.00481	2–7	0.01783	6.90
1–3	0.00543	1–4	0.00474	2–8	0.00824	23.42
1–3	0.00543	1–5	0.00481	2–9	0.00826	23.97
1–4	0.00474	1–5	0.00481	2–10	0.00705	35.46

stresses, and these 10 sets in Table 4 cover every combination of 2 stresses.

The stress levels in test 2–1 to 2–10 correspond to those in test 1–1 to 1–5. For example, the two accelerated stress levels in 2–1 are designed to be the combination of accelerated stress levels in 1–1 and 1–2 to explore the relationship between temperature and discharge rate.

2.3. Parameter recognition experiments of single-factor models

Further experiments were carried out on 6 new cells of the same kind as those in Section 2.1 to identify the parameters in Eqs. (3)–(7).

3. Experiment results

3.1. Results of the single factor accelerated experiments

The cycling curves of test 1–2 in Table 3 are shown in Fig. 1 as an example of all the single-factor accelerated experiments. Only parts of curves are plotted because many cycles were completed.

The capacity of each cycle and the standard capacity after every 20 cycles can be calculated according to the cycling discharge curves and the standard capacity tests, while the ohmic resistance and total resistance can be measured by the HPPC method after every 20 cycles. The cycling capacity, the standard capacity and the resistances are shown in Fig. 2, and the ohmic resistance and total resistance during discharge and charge are noted as $R_{dch-ohm}$, $R_{dch-tot}$, $R_{cha-ohm}$ and $R_{cha-tot}$ in the figure.

The fitted line of each standard capacity curve in Fig. 2 is assumed to have the form $y = a - fx$. This equation describes the relationship between the standard capacity y, the cycling times x and the capacity fade rate f, where α is the initial capacity when $x = 0$. Thus, the standard capacity fade rate (SCFR) is defined as follows: $f = (a - y)/x$, with a unit of Ah(cycle)$^{-1}$.

The SCFR of all single-factor experiments are shown in Table 5.

3.2. Results of the double-factor accelerated experiments

The cycling curves of test 2–3 in Table 4 are shown in Fig. 3 to represent all the double-factor accelerated experiments. Only partial curves are plotted due to the large number of cycles.

The cycling capacity, the standard capacity and the resistance for each test in Table 4 are shown in Fig. 4.

The SCFR of all double-factor experiments are shown in Table 5.

Test 2–1 in Table 4 only cycled 60 times due to a sharp decline in its cycling capacity under 45 °C with a 4 C discharge rate. After extending its rest time from 5 min to 2 h, the rapid decay eased, as shown in Fig. 4(a). However, after 60 cycles, the cycling capacity remained less than 2 Ah. To ensure the safety of laboratory personnel and equipment, the cycling experiment was stopped after the 60th cycle.

4. Analysis of the experimental results

The slopes of linear fit lines to the standard capacity degradation, namely, the SCFR, are listed in Table 5 with a unit of Ah(cycle)$^{-1}$.

The coupling errors in Table 5 are calculated by Eq. (1):

$$\Delta = \frac{\sum_{i=1}^{2} SCFR_i - SCFR_d}{SCFR_d} \times 100\% \quad (1)$$

where $\sum_{i=1}^{2} SCFR_i$ is the sum of the SCFR values of 2 single-factor tests and $SCFR_d$ is the SCFR of the corresponding double-factor test listed in the same row in Table 5.

The coupling errors in Table 5 reveal significant information about the joint effect of these 5 influential factors:

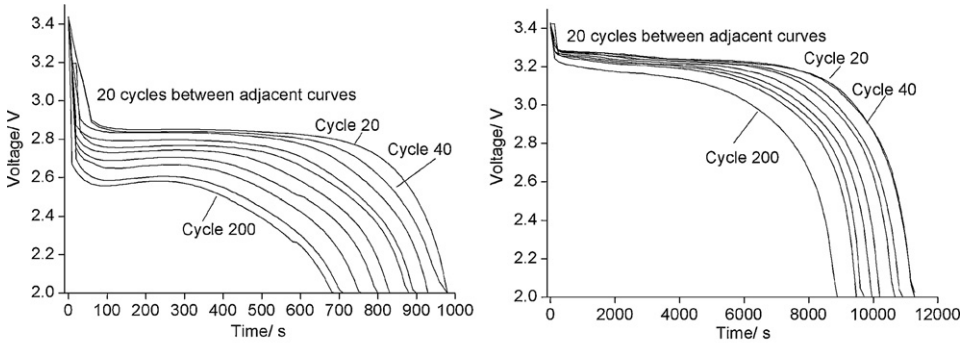

Fig. 1. Test No. 1–2 cycling discharge curves (partial) and standard capacity tests.

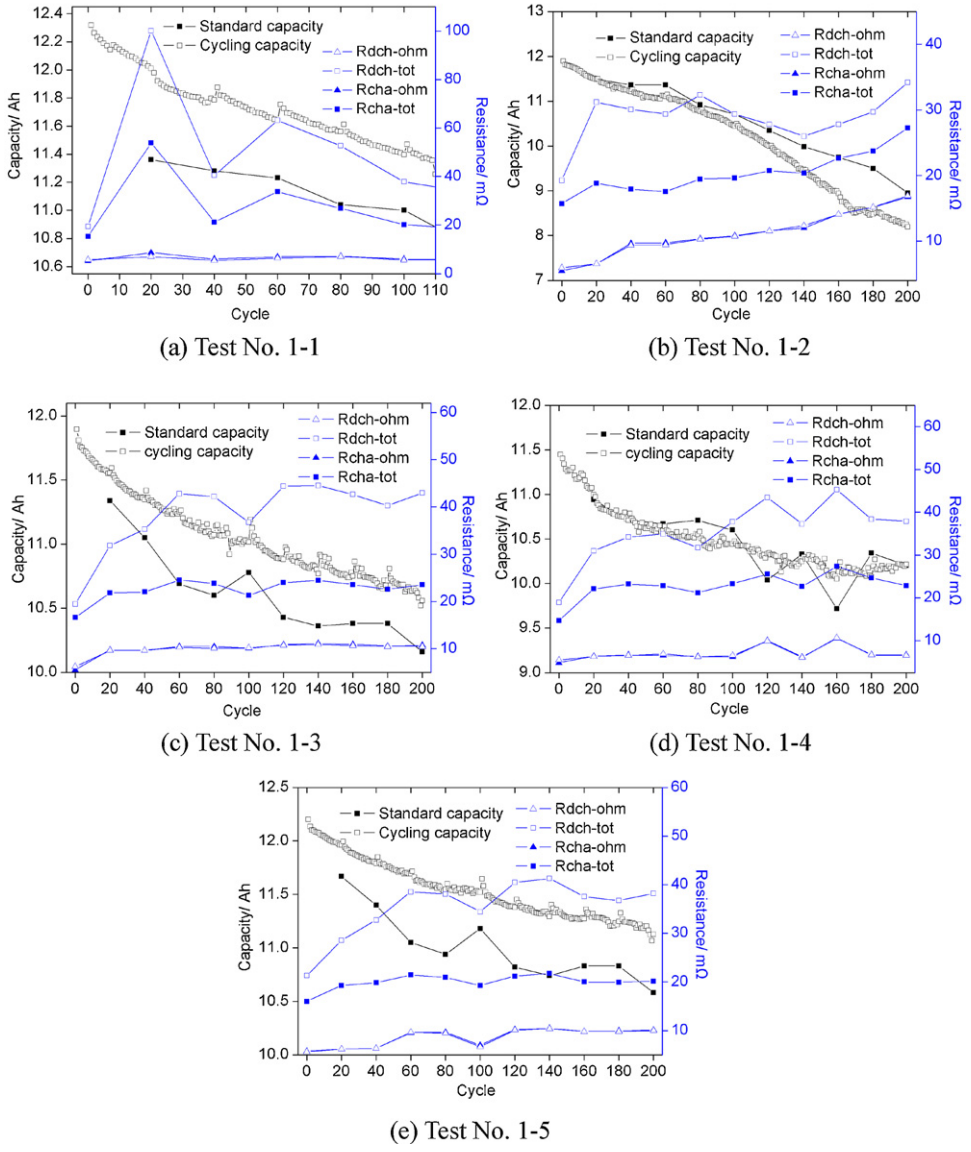

Fig. 2. (a)–(e) The cycling capacity, the standard capacity and the resistances of single factor accelerated experiments.

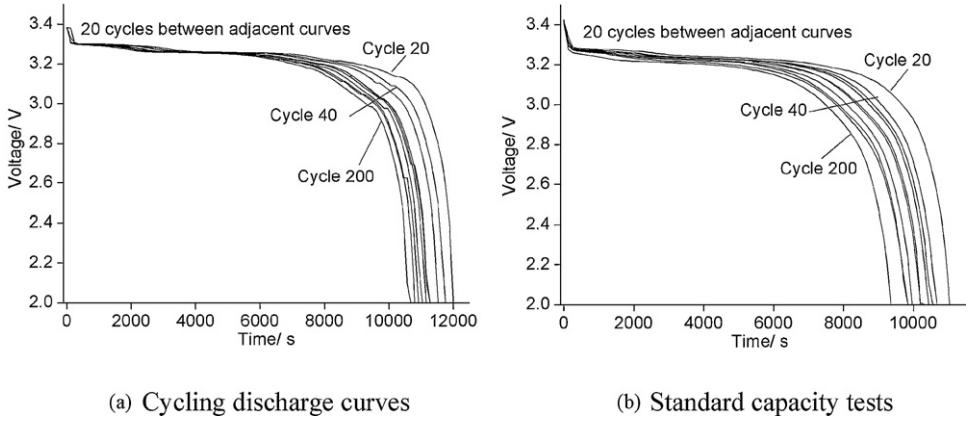

Fig. 3. Test No. 2–3 cycling discharge curves (partial) and standard capacity tests.

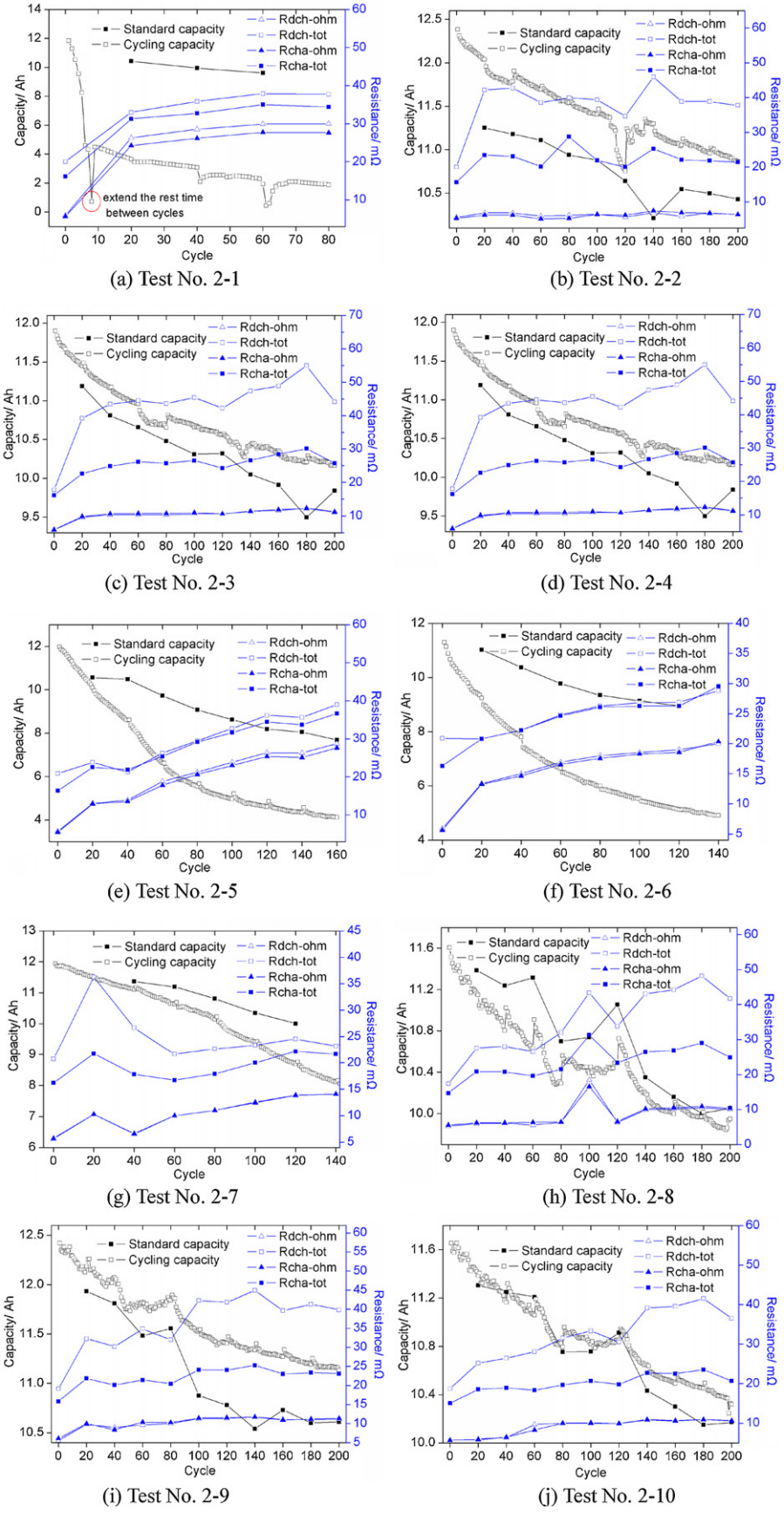

Fig. 4. (a)–(j) The cycling capacity, the standard capacity and the resistance of double-factor accelerated experiments.

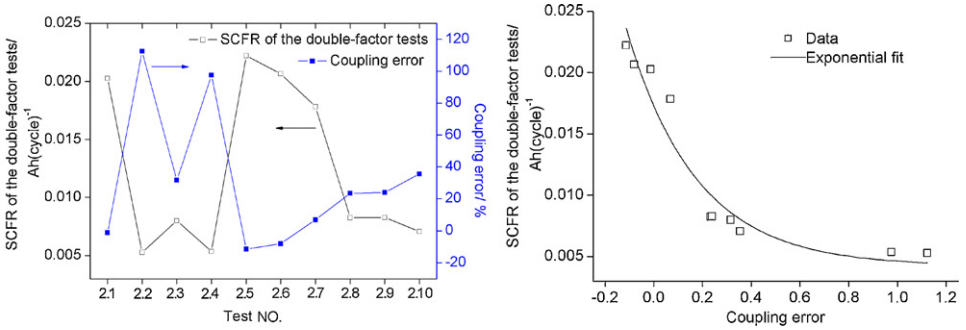

(a) The reverse trend (b) The exponential fit

Fig. 5. The relationship between Δ and $SCFR_d$.

(1) The value of the coupling error reflects the error of the entirely-decoupled assumption compared with the real situation. Table 5 shows that there is coupling between almost every set of two stresses. Neglecting coupling considerably will reduce the model accuracy due to the relatively large coupling errors, as shown in the table.
(2) The Δ and $SCFR_d$ in Table 5 demonstrate an obvious reverse trend and fit an exponential decay relationship with a coefficient of determination $R^2 = 0.94$, as shown in Fig. 5(a) and (b). Although the determination coefficient of the fitting is not perfect, because it is impossible (and not required) to forecast the battery lifespan as accurately as 1 month or several days, the accuracy of the battery degradation prediction model is far below the general requirements in dynamic controls. Therefore, this fitting coefficient is acceptable.

Based on the lack of one-time damages, as $SCFR_d$ increases, the coupling error approaches a negative value. The coupling error equals zero at a critical $SCFR_d$; thus, the two factors are completely decoupled and affect battery degradation separately. When the $SCFR_d$ is less than the critical value, the coupling error is positive, and the interaction between the two factors reduces the degradation of the battery. When the $SCFR_d$ is greater than the critical value, the coupling error is negative, and the degradation becomes more intense due to the interaction between these two factors. Therefore, the impact of coupling on battery capacity can be obtained from the stress level input.
(3) When the stress levels are beyond the normal scope, the capacity fading mechanism might change; thus, Fig. 5(b) should be applied in a limited range. The applicable range is derived in the following modeling process.

5. Model development

5.1. Model derivation

For a battery capacity degradation model with five independent stresses as input, the SCFR under joint effect can be expressed as follows:

$$SCFR_0 = SCFR_T + SCFR_{DR} + SCFR_{EODV} + SCFR_{CR} + SCFR_{EOCV} \quad (2)$$

where $SCFR_T$, $SCFR_{DR}$, $SCFR_{EODV}$, $SCFR_{CR}$ and $SCFR_{EOCV}$ refer to the SCFR when the single stress accelerated input is temperature, discharge rate, EODV, charge rate and EOCV, respectively.

Several single stress durability models, such as the Arrhenius and Inverse Power Law models [21,22], have been developed and can be applied to describe the relationship between battery lifespan and single factors:

$$SCFR_T = \frac{b}{\xi_T} = \frac{b}{A_T e^{C_T/T}} \quad (3)$$

$$SCFR_{DR} = \frac{b}{\xi_{DR}} = \frac{b}{B_{DR} I_{DR}^{-D_{DR}}} \quad (4)$$

$$SCFR_{EODV} = \frac{b}{\xi_{EODV}} = \frac{b}{B_{EODV} \nu_{EODV}^{-D_{EODV}}} \quad (5)$$

$$SCFR_{CR} = \frac{b}{\xi_{CR}} = \frac{b}{B_{CR} I_{CR}^{-D_{CR}}} \quad (6)$$

$$SCFR_{EOCV} = \frac{b}{\xi_{EOCV}} = \frac{b}{B_{EOCV} \nu_{EOCV}^{-D_{EOCV}}} \quad (7)$$

where ξ_T, ξ_{DR}, ξ_{EODV}, ξ_{CR}, and ξ_{EOCV} are the cycle life when the single stress accelerated input is temperature, discharge rate, EODV, charge rate and EOCV, respectively; A_T, B_{DR}, B_{EODV}, B_{CR}, and B_{EOCV} are the constant parameters before the power function, and C_T, D_{DR}, D_{EODV}, D_{CR}, and D_{EOCV} are the constant parameters in the power function. T is the temperature in K; I_{DR} and I_{CR} are the discharge and charge rate; ν_{EODV} and ν_{EOCV} are the EODV and EOCV; b is defined as $b = a - y_{sec}$, in which y_{sec} is the standard capacity when the battery life ends.

Thus, Eq. (2) can be substituted by:

$$\xi_0 = \frac{b}{SCFR_0} = \left(\frac{1}{A_T e^{C_T/T}} + \frac{1}{B_{DR} I_{DR}^{-D_{DR}}} + \frac{1}{B_{EODV} \nu_{EODV}^{-D_{EODV}}} + \frac{1}{B_{CR} I_{CR}^{-D_{CR}}} + \frac{1}{B_{EOCV} \nu_{EOCV}^{-D_{EOCV}}} \right)^{-1} \quad (8)$$

where ξ_0 is the cycle life under five independent accelerated stresses.

Then, this model is modified to take into account the coupling between stresses according to the coupling error analysis performed in Section 4:

$$\begin{aligned} SCFR_0{}^c = {} & \frac{\partial_1}{4}(SCFR_T + SCFR_{DR}) + \frac{\partial_2}{4}(SCFR_T + SCFR_{EODV}) + \frac{\partial_3}{4}(SCFR_T + SCFR_{CR}) + \frac{\partial_4}{4}(SCFR_T + SCFR_{EOCV}) \\ & + \frac{\partial_5}{4}(SCFR_{DR} + SCFR_{EODV}) + \frac{\partial_6}{4}(SCFR_{DR} + SCFR_{CR}) + \frac{\partial_7}{4}(SCFR_{DR} + SCFR_{EOCV}) + \frac{\partial_8}{4}(SCFR_{EODV} + SCFR_{CR}) \\ & + \frac{\partial_9}{4}(SCFR_{EODV} + SCFR_{EOCV}) + \frac{\partial_{10}}{4}(SCFR_{CR} + SCFR_{EOCV}) \end{aligned} \quad (9)$$

where $SCFR_0{}^c$ is the $SCFR_0$ after considering stress coupling. ∂_1, $\partial_2 \ldots \partial_{10}$ are the coupling correction factors between every 2

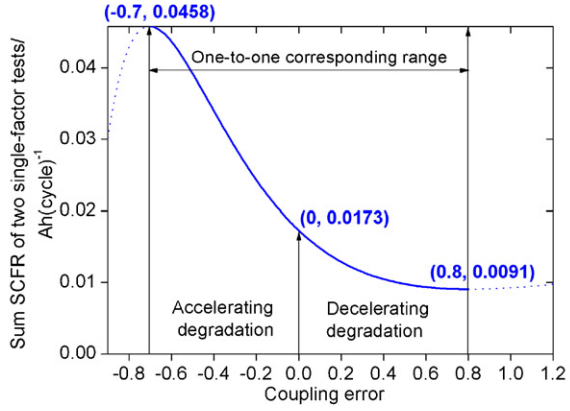

Fig. 6. The relationship between coupling error and the two single-factor SCFR.

stresses. Each of the factors equals 1 and Eq. (9) is transformed to Eq. (2) under the assumption of complete decoupling.

An example of how to calculate ∂_1 is given to illustrate the calculation method for all the coupling correction factors.

(1) ∂_1 is the coupling correction factor of the stress of temperature and discharge rate, and Eq. (1) is applied to obtain the coupling error of this combination:

$$\Delta_{\partial 1} = \frac{SCFR_T + SCFR_{DR} - SCFR_{T-DR}}{SCFR_{T-DR}} \times 100\% \quad (10)$$

where $SCFR_{T-DR}$ is the $SCFR_d$ with temperature and discharge rate as double accelerated stresses. $SCFR_T$ and $SCFR_{DR}$ in this formula is calculated from Eqs. (3) and (4).

(2) Eq. (11), which is obtained from the exponential fitting of Fig. 5(b), provides another formula for $\Delta_{\partial 1}$ and $SCFR_{T-DR}$ in addition to Eq. (10).

$$SCFR_{T-DR} = 0.01306e^{-\Delta_{\partial 1}/0.28794} + 0.00422 \quad (11)$$

The relationship between $\Delta_{\partial 1}$ and $(SCFR_T + SCFR_{DR})$ derived from Eqs. (10) and (11) is shown in Fig. 6.

In Fig. 6, when Δ is in the range of $[-0.7, 0.8]$, Δ and $(SCFR_T + SCFR_{DR})$ have one-to-one correspondence, and $(SCFR_T + SCFR_{DR})$ is in the range of $[0.0091, 0.0458]$.

When $(SCFR_T + SCFR_{DR}) \in [0.0091, 0.0173)$
$\Rightarrow \Delta \in (0,\ 0.8]$
$\Rightarrow (SCFR_T + SCFR_{DR}) > SCFR_{T-DR}$, the coupling between factors lessens the battery capacity fade.
When $(SCFR_T + SCFR_{DR}) \in (0.0173, 0.0458]$
$\Rightarrow \Delta \in [-0.7, 0)$
$\Rightarrow (SCFR_T + SCFR_{DR}) < SCFR_{T-DR}$, the coupling between factors speeds up the battery capacity fade.

When the stress is too large or small, the sum of two single-factor SCFR may fall outside the one-to-one correspondence range. If the stress is not far off the one-to-one interval, its corresponding coupling error can be calculated through linear extrapolation based on the start and end points of the interval. If the deviation is higher, the battery fading mechanism may have been changed, and the above rules may be no longer applicable.

Because the range outside the one-to-one interval exceeds the experimental scope in Section 3, it can only be concluded that if the stress is in the right lateral region of the one-to-one interval, the stress level is extremely small, the coupling between factors significantly reduces the battery fade, and the SCFR under double-factor conditions is much smaller than the sum of the fading rates of the two single-factor experiments. Therefore, the coupling error is so big that the correction factor in Eq. (12) is close to zero. Similarly, if the stress is in the left lateral region, the coupling error tends to -1, and the correction factor tends to positive infinity.

Given the stress levels of each of two single factors, the coupling error can be calculated by the look-up table provided in Fig. 6.

(3) Since ∂_1 is defined as the ratio of $SCFR$ under double-factor conditions to its corresponding sum under two single-factor conditions, it can be written as follows:

$$\partial_1 = \frac{SCFR_{T-DR}}{SCFR_T + SCFR_{DR}} = \frac{1}{1 + \Delta_{\partial 1}} \quad (12)$$

(4) ∂_1 can be solved using Eqs. (10), (11) and (12) together. Similar methodology can be applied to the derivation of other coupling correction factors, and $SCFR_0^c$ in Eq. (9) can be calculated to predict the cycle life under multi-stress accelerated conditions:

$$\xi_0^c = \frac{b}{SCFR_0^c} \quad (13)$$

5.2. Parameter recognition and model accuracy validation

Model parameters are identified and the model accuracy is verified through cycling tests in this section.

First, the battery life is assumed to end when the standard capacity declines to 70% of nominal capacity. Thus,

$$b = a - y_{sec} = 11 \times (1 - 70\%) = 3.3\,\text{Ah}$$

Second, several extra single-factor experiments are conducted to determine the SCFR, which can be used in the model parameters identification of Eqs. (3)–(7). The parameters in Eqs. (3)–(7) determined from these experiments are shown in Table 6.

Then, a test is carried out with the conditions shown in Table 7 to verify the model accuracy.

If each stress in Table 7 occurs while the other stresses remain at the standard levels, the SCFR of these five single-factor accelerated experiments are counted in Table 8 according to the parameter recognition results in Table 6 and the inputs in Table 7.

The corresponding coupling errors and correction factors between the factors in Table 7 are calculated and shown in Table 9 using the look-up curve in Fig. 6.

Table 6
Parameter recognition results for single-factor Eqs. (3)–(7).

$SCFR$	Multiplier factor parameters	Power parameters
$SCFR_T$	$A_T = 0.0635$	$C_T = 2838.0121$
$SCFR_{DR}$	$B_{DR} = 624.8817$	$D_{DR} = 0.6905$
$SCFR_{EODV}$	$B_{EODV} = 547.8087$	$D_{EODV} = 0.8514$
$SCFR_{CR}$	$B_{CR} = 641.6489$	$D_{CR} = 0.4754$
$SCFR_{EOCV}$	$B_{EOCV} = 7.6638 \times 10^5$	$D_{EOCV} = 5.1960$

Table 7
Model accuracy test.

Test parameter items	Parameter value and unit
Ambient temperature	50 °C
Discharge rate	1/3 C
EODV	2 V
Charge rate	1/3 C
EOCV	4.2 V
Cycling times	110
SFCR	0.01337

Table 8
SCFR of single-factor accelerated experiments under the input of Table 7.

$SCFR_T$	$SCFR_{DR}$	$SCFR_{DR}$	$SCFR_{CR}$	$SCFR_{EOCV}$
0.0079	0.0025	0.0033	0.0030	0.0075

Table 9
The coupling errors and correction factors using the input values shown in Table 7.

Correction factor symbol	Sum of two single-factor SCFR	Coupling error	Correction factors
∂_1	0.0104	0.41	0.7092
∂_2	0.0112	0.32	0.7576
∂_3	0.0109	0.35	0.7407
∂_4	0.0154	0.07	0.9346
∂_5	0.0058	NA[a]	0
∂_6	0.0055	NA	0
∂_7	0.01	0.47	0.6803
∂_8	0.0063	NA	0
∂_9	0.0108	0.36	0.7353
∂_{10}	0.0105	0.4	0.7143

[a] Both of the stress levels are quite small, and the stress level is to the right of the one-to-one interval; thus, the correction factor can be assumed to be approximately zero.

Finally, the results in Tables 8 and 9 can be substituted into Eq. (9), and the SCFR under the joint effect of 5 factors, which has taken into stress coupling into account, can be calculated as follows:

$SCFR_{cou} = 0.0151.$

The SCFR without considering stress coupling is counted by the sum of all single-factor SCFR in Table 8:

$SCFR_{decou} = 0.0242.$

Compared with the real experimental result of the SCFR in Table 7 ($SCFR_{real}$ = 0.01337), the SCFR value without accounting for stress coupling ($SCFR_{decou}$) caused a forecast error of 81%, whereas the $SCFR_{cou}$, derived from the capacity degradation model that has been modified by stress coupling, achieved an error less than 12.94%. The three SCFR are compared in Fig. 7.

With the ongoing cycling of the experiment in Table 7, the $SCFR_{real}$ obtained by the known data is gradually changing. Fig. 8 shows that the model error fluctuates with an increasing number of cycles. It can be concluded that for the first few dozen cycles, the model error can be up to 50% due to fluctuation of the capacity fading rate; when the cycle number accumulates to 60 or more, the absolute value of the model error is reduced to less than 20%. When the cycle number increases to 110, the model error is approximately 13%. The error converges non-monotonically as the cycling continues, which is relevant to the stabilization of the standard capacity fading rate as the number of cycles increases.

5.3. Factor sensitivity analysis

The capacity degradation model provides an analysis tool to explore the sensitivity of battery durability to these five factors, and

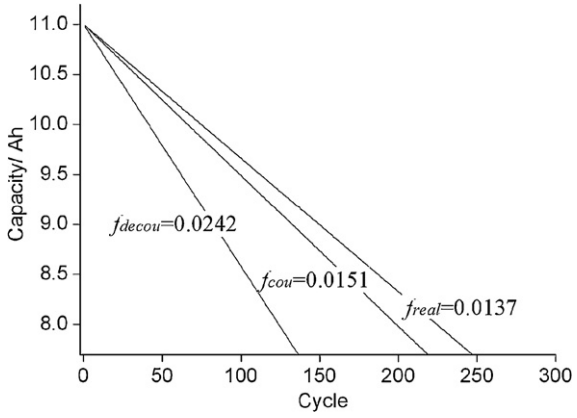

Fig. 7. SCFR comparison.

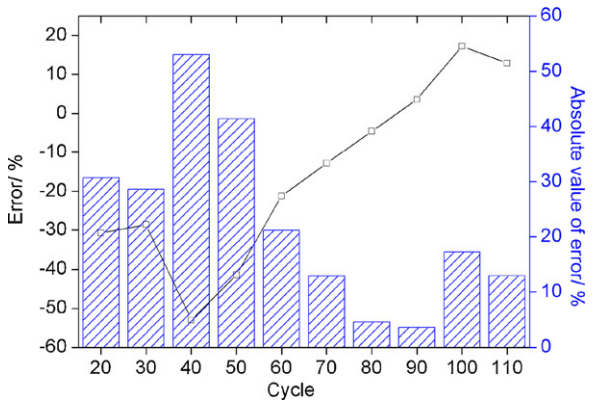

Fig. 8. Error convergence of the durability model.

the relationship between SCFR and the five factors can be obtained from the derivative of Eq. (9).

$$\frac{\partial SCFR_0^c}{\partial T} = \frac{\partial SCFR_0^c}{\partial SCFR_T} \cdot \frac{\partial SCFR_T}{\partial T} = \frac{(\partial_1 + \partial_2 + \partial_3 + \partial_4)}{4} \cdot \frac{b}{A_T} e^{-C_T/T} \cdot \frac{C_T}{T^2} \quad (14)$$

$$\frac{\partial SCFR_0^c}{\partial I_{DR}} = \frac{\partial SCFR_0^c}{\partial SCFR_{DR}} \cdot \frac{\partial SCFR_{DR}}{\partial I_{DR}} = \frac{(\partial_1 + \partial_5 + \partial_6 + \partial_7)}{4} \cdot \frac{b}{B_{DR}} \cdot D_{DR}(I_{DR})^{D_{DR}-1} \quad (15)$$

$$\frac{\partial SCFR_0^c}{\partial v_{EODV}} = \frac{\partial SCFR_0^c}{\partial SCFR_{EODV}} \cdot \frac{\partial SCFR_{EODV}}{\partial v_{EODV}} = \frac{(\partial_2 + \partial_5 + \partial_8 + \partial_9)}{4} \cdot \frac{b}{B_{EODV}} \cdot (-D_{EODV})(v_{EODV})^{-D_{EODV}-1} \quad (16)$$

$$\frac{\partial SCFR_0^c}{\partial I_{CR}} = \frac{\partial SCFR_0^c}{\partial SCFR_{CR}} \cdot \frac{\partial SCFR_{CR}}{\partial I_{CR}} = \frac{(\partial_3 + \partial_6 + \partial_8 + \partial_{10})}{4} \cdot \frac{b}{B_{CR}} \cdot D_{CR}(I_{CR})^{D_{CR}-1} \quad (17)$$

$$\frac{\partial SCFR_0^c}{\partial v_{EOCV}} = \frac{\partial SCFR_0^c}{\partial SCFR_{EOCV}} \cdot \frac{\partial SCFR_{EOCV}}{\partial v_{EOCV}} = \frac{(\partial_4 + \partial_7 + \partial_9 + \partial_{10})}{4} \cdot \frac{b}{B_{EOCV}} \cdot D_{EOCV}(v_{EOCV})^{D_{EOCV}-1} \quad (18)$$

The following condition is adopted as an example to analyze the factor sensitivity of the durability model: ambient temperature of 40 °C, a discharge rate of 3 C, EODV of 1.5 V, a charge rate of 1 C, and EOCV of 4 V. The coupling errors and the correction factors under this condition are calculated and shown in Table 10.

Given the parameter identification in Table 6 and the correction factors in Table 10, the result of the capacity fading rate of this sensitivity analysis case is around 0.0338, based on Eq. (9). The derivative results in Table 11 are obtained by calculating Eqs. (14)–(18).

Sensitivity analysis can help determine the maximum-weighted influence factors for battery life. Here, the concept of 'equivalent stress increment' is introduced to describe a group of factor increments that affect battery life equivalently. The variables ΔT, ΔI_{DR}, Δv_{EODV}, ΔI_{DC} and Δv_{EOCV} in the following formula form a group of

Table 10
The coupling errors and correction factors for the case of factor sensitivity analysis.

Correction factor symbol	Sum of two single-factor SCFR	Coupling error	Correction factors
∂_1	0.0173	0	1
∂_2	0.0145	0.12	0.8929
∂_3	0.0111	0.33	0.7519
∂_4	0.0118	0.28	0.7813
∂_5	0.0198	−0.08	1.0870
∂_6	0.0164	0.03	0.9709
∂_7	0.0171	0.01	0.9901
∂_8	0.0137	0.16	0.8621
∂_9	0.0143	0.13	0.8850
∂_{10}	0.0109	0.35	0.7407

Table 11
The derivative results for factor sensitivity analysis.

$\frac{\partial SCFR_0^c}{\partial T}$	$\frac{\partial SCFR_0^c}{\partial I_{DR}}$	$\frac{\partial SCFR_0^c}{\partial v_{EODV}}$	$\frac{\partial SCFR_0^c}{\partial I_{DC}}$	$\frac{\partial SCFR_0^c}{\partial v_{EOCV}}$
1.488×10^{-4}	0.0026	−0.0022	0.0020	0.0064

equivalent stress increments to battery life.

$$\frac{\partial SCFR_0^c}{\partial T}\Delta T = \frac{\partial SCFR_0^c}{\partial I_{DR}}\Delta I_{DR} = \frac{\partial SCFR_0^c}{\partial v_{EODV}}\Delta v_{EODV} = \frac{\partial SCFR_0^c}{\partial I_{CR}}\Delta I_{CR} = \frac{\partial SCFR_0^c}{\partial v_{EOCV}}\Delta v_{EOCV} \quad (19)$$

A group of equivalent stress increments, as in Eq. (20), are calculated from the derivatives in Table 11.

$$\begin{cases} \Delta T = 10\ ^\circ\mathrm{C} \\ \Delta I_{DR} = 0.5722\,\mathrm{C} \\ \Delta v_{EODV} = -0.6762\,\mathrm{V} \\ \Delta I_{CR} = 0.7439\,\mathrm{C} \\ \Delta v_{EOCV} = 0.2325\,\mathrm{V} \end{cases} \quad (20)$$

The group of equivalent stress increments indicates that each one of the following events will have an equivalent impact on battery life: a temperature increase of 10 °C, a discharge rate increase of 0.57 C, an EODV decrease of 0.68 V, a charge rate increase of 0.74 C and an EOCV increase of 0.23 V. Hence, the following conclusions on the model sensitivity can be drawn:

(1) The ambient temperature significantly affects battery life. Taking the cycling conditions of the sensitivity analysis as the starting point, a 10 °C rise in temperature will increase the capacity fading rate by 0.0015 and shorten the calendar life by 5%. As with cycling under high temperature, cycling under low temperatures also accelerates the degradation of batteries. The natural temperature range is as wide as 40 °C in Beijing from summer to winter, and a proper heating and cooling system for battery packs will help achieve a longer battery life.
(2) The battery life will be shortened by a too low EODV or too high EOCV, and the sensitivity to EOCV is significantly higher than to EODV. In the above example, the 0.23 V increase of EOCV has an equivalent impact on battery life to a 0.68 V drop of EODV. Compared to over-discharge, over-charge is more likely to be a fatal mistake for lithium-ion batteries, and the charging process should be carefully controlled.
(3) Excessive charge and discharge rates harm batteries, and battery life is more sensitive to discharge rate than to charge rate. In the above example, increasing the discharge rate by 0.57 C is equivalent to increasing the charge current by 0.74 C. Additionally, the standard charge is more favorable for batteries than the fast charge. Given the same operating conditions, including the same EOCV, if the standard charge rate (e.g., 1/3 C) is changed to a fast charge rate (e.g., 3 C), the battery life will be shortened by more than 20%.

It should be noted that the stress increments in formula (20) are based on the starting point of the conditions in this sensitivity analysis. The data in Eq. (20) and in the above conclusions are subject to change when the starting point has been altered.

6. Conclusions

A battery capacity degradation model with the multi-factor input is studied in this paper. First, durability tests are performed to obtain the capacity fade and resistance increase with cycling and to verify the general existence of coupling between stresses. According to the coupling verification test results, the relevance between coupling intensity and stress levels is further investigated. Then, the multi-factor capacity degradation model is established based on the coupling intensity calibration and the input of real operating conditions. This model achieves an error less than 15% when the cycling goes into the stable decay period, and the error converges gradually as the cycling continues. Finally, model sensitivity analysis was performed to determine the different weights of these five factors with respect to battery life.

The main conclusions of this paper are as follows:

(1) The 5 influencing factors of battery capacity degradation, which are ambient temperature, discharge rate, EODV, charge rate, and EOCV, are coupled in general.
(2) The coupling is related to stress levels. There exists a critical stress level at which the coupling can be relatively neglected. When the stress level exceeds the critical value, the coupling aggravates the battery degradation exponentially.
(3) Battery life is significantly affected by the ambient temperature, the too low EODV or too high EOCV, and the excessive charge and discharge rates. Battery life shows stronger sensitivity to discharge rate and EOCV than to charge rate and EODV. In addition, the standard charge is more favorable for battery durability than the fast charge.

This degradation model alleviates the problem of poor accuracy in models that do not consider coupling and demonstrates a preferable adaptability to the complexity of the multi-factor input. The application of the model requires only the calibration of coupling characteristics and the input of real-time operating conditions, which ensures easy applicability to batteries on electric appliances and vehicles.

Acknowledgements

This work is supported by the MOST (Ministry of Science and Technology) of China under contract No. 2010DFA72760 (Collaboration on Cutting-edge Technology Development of Electric Vehicle between US and China) and the Delta Science & Technology Educational Development Program.

References

[1] H. Wenzl, I. Baring-Gould, R. Kaiser, et al., J. Power Sources 144 (2005) 373–384.
[2] D.U. Sauer, H. Wenzl, J. Power Sources 176 (2008) 534–546.
[3] J. Vetter, P. Novak, M.R. Wagner, et al., J. Power Sources 147 (2005) 269–281.
[4] G. Ning, R.E. White, B.N. Popov, Electrochim. Acta 51 (2006) 2012–2022.
[5] R. Spotnitz, J. Power Sources 113 (2003) 72–80.
[6] J. Li, E. Murphy, J. Winnick, et al., J. Power Sources 102 (2001) 302–309.
[7] M.C. Smart, B.V. Ratnakumar, L.D. Whitcanack, et al., J. Power Sources 119-121 (2003) 349–358.
[8] P. Ramadass, B. Haran, R. White, et al., J. Power Sources 112 (2002) 606–613.

[9] P. Ramadass, B. Haran, R. White, et al., J. Power Sources 112 (2002) 614–620.
[10] Y. Kida, A. Kinoshita, K. Yanagida, et al., Electrochim. Acta 47 (2002) 1691–1696.
[11] M. Broussely, P. Biensan, F. Bonhomme, et al., J. Power Sources 146 (2005) 90–96.
[12] C.S. Wang, X.W. Zhang, A.J. Appleby, et al., J. Power Sources 112 (2002) 98–104.
[13] B.V. Ratnakumar, M.C. Smart, S. Surampudi, J. Power Sources 97–98 (2001) 137–139.
[14] X.F. Meng, Z.P. Wang, High Technol. Lett. 16 (2010) 13–17.
[15] P. Spagnol, S. Onori, N. Madella, et al., Aging and characterization of Li-ion batteries in a HEV application for lifetime estimation, in: 6th IFAC Symposium: Advances in Automotive Control, Munich, Germany, 2010.
[16] K. Takei, K. Kumai, Y. Kobayashi, J. Power Sources 97–98 (2001) 697–701.
[17] I. Bloom, B.W. Cole, J.J. Sohn, et al., J. Power Sources 101 (2001) 238–247.
[18] Y.C. Zhang, C.Y. Wang, X.D. Tang, J. Power Sources 196 (2011) 1513–1520.
[19] J. Wang, P. Liu, J.H. Garner, et al., J. Power Sources 196 (2011) 3942–3948.
[20] FreedomCAR Battery Test Manual for Power-Assist Hybrid Electric Vehicles. INEEL, October, 2003.
[21] Z.H. Zhang, Accelerated Life Testing and Statistical Analysis, Beijing University of Technology Press, Beijing, 2002.
[22] S.S. Mao, L.L. Wang, Accelerated Life Testing, Science Press, Beijing, 2000.